Plasmonic Ag@Oxide Nanoprisms for Enhanced Performance of Organic Solar Cells

*Peng Du, Pengtao Jing, Di Li, Yinghui Cao, Zhenyu Liu, and Zaicheng Sun**

Localized surface plasmon resonance (LSPR), light scattering, and lowering the series resistance of noble metal nanoparticles (NPs) provide positive effect on the performance of photovoltaic device. However, the exciton recombination on the noble metal NPs accompanying above influences will deteriorate the performance of device. In this report, surface-modified Ag@oxide (TiO_2 or SiO_2) nanoprisms with 1–2 nm shell thickness are developed. The thin film composed of P3HT/Ag@oxides and P3HT:PCBM/Ag@oxides is investigated by absorption, photoluminescence (PL), and transient absorption spectroscopy. The results show a significant absorption, PL enhancement, and long-lived photogenerated polaron in the P3HT/Ag@TiO_2 film, indicating the increase of photogenerated exciton population by LSPR of Ag nanoprisms. In the case of P3HT/Ag nanoprisms, partial PL quench and relatively short-lived photogenerated polaron are observed. That indicates that the oxides layer can effectively avoid the exciton recombination. When the Ag@oxide nanoprisms are introduced into the active layer of P3HT:PCBM photovoltaic devices, about 31% of power conversion efficiency enhancement is obtained relative to the reference cell. All these results indicate that Ag@oxides can enhance the performance of the cell, at the same time the ultrathin oxide shell prevents from the exciton recombination.

P. Du, Dr. P. Jing, Dr. D. Li, Prof. Z. Sun
State Key Laboratory of Luminescence and Applications
Changchun Institute of Optics
Fine Mechanics and Physics
Chinese Academy of Sciences
3888 East Nanhu Road, Changchun,
Jilin 130033, P.R. China
E-mail: sunzc@ciomp.ac.cn

P. Du
University of Chinese Academy of Sciences
Beijing 100000, P.R. China

Dr. Y. Cao, Prof. Z. Liu
State Key Laboratory of Applied Optics
Changchun Institute of Optics
Fine Mechanics and Physics
Chinese Academy of Sciences
3888 East Nanhu Road, Changchun, Jilin 130033, P.R. China

DOI: 10.1002/smll.201402757

1. Introduction

Bulk heterojunction (BHJ) organic photovoltaic devices (OPVs) with bicontinuous networks of a polymer/fullerene derivatives have been intensely studied because of their attractive properties such as light weight, high flexibility, low-temperature, solution-based processability, and so on.[1] Researchers have devoted most of their efforts on pursuing organic solar cells with high power conversion efficiency (PCE), such as design and synthesis of low bandgap molecules and polymer with a broad light absorption,[2] optimization of the device structures,[3] and improvement of the active layer morphology, etc.[4] To date, OPV devices have exhibited PCE exceeding 10%.[5] However, most molecular and polymeric materials have low charge-carrier mobility and short exciton diffusion length, limiting the devices thickness within a few hundred nanometers and leading to a poor solar light absorption.[6] That results in insufficient photo-generated carriers

small NANO MICRO

generation and collection. The localized surface plasmon resonance (LSPR) effect of noble metal nanoparticles (NPs) (Au and Ag NPs and other metallic nanostructures) could be regarded as an effective way to improve the PCE of solar cell.[7] Noble metal nanostructures could enhance the incident light energy in the vicinity of the nanostructure and improve the photogeneration of excitons.[8] Typically, the metal NPs are either embedded in the charge-transfer layer such as PEDOT:PSS or simply blended within the active layer of OPV. However, the findings from these approaches are highly controversial as both enhancement[6,9] and detraction[10] in OPV devices' performance have been reported. Wang et al. found that the increase of PCE strongly depend on the size and weight fraction of Au NPs, which embedded in the active layer of OPV device.[6b] However, it is hard to attribute that the LSPR effect of Au NPs is a dominant factor for the PCE enhancement. Xue et al. reported that the addition of Ag NPs into the active layer significantly enhanced the local absorption and the carrier mobility but depressed the total extracted carriers.[10c] Although large amount of carriers move on a subnetwork of Ag NPs, those could not be completely extracted before they undergo recombination on the Ag NPs, as traps, leading to monomolecular recombination. Therefore, light scattering, LSPR, carrier mobility, and charge-carrier recombination are involved in PCE enhancement of solar cells. The former three factors provide positive contribution, while carrier recombination, which involves metal NPs, gives a negative effect.[10a] In order to better use of LSPR effect in BHJ OPVs, refraining exciton from recombination is an effective way to boost PCE of solar cells.

In our previous reports, we successfully synthesized Ag nanoprisms coated with ultrathin oxide layer to form Ag@oxide core–shell structure.[11] The oxide layer could not only improve the stability of Ag nanoprisms, but also effectively prevent the photogenerated charges from recombination. Ag@oxide core–shell nanoprisms were introduced underneath P3HT thin film, about 34% absorption enhancement was observed. It should be noted that the LSPR effect quickly attenuates along the distance (10–20 nm) away from NP surface. It requires that the shell thickness is as thin as possible to maximize the LSPR performance. However, the LSPR effect still contributes within a narrow domain (≈20 nm) for bilayer device. Embedding Ag@oxides nanoprisms within active layer offers a highly convenient approach for integrating plasmonic entities in organic solar cells. Herein, we surface-modified the Ag@oxides nanoprism via alkyl groups via physical or chemical route to make Ag@oxides nanoprisms well dispersed into active layer—poly (3-hexylthiophene):[6,6]-phenyl-C 61-butyric acid methyl ester (P3HT:PCBM). Atomic force microscopy (AFM) images show that the morphology of thin film has slightly changed when the Ag@oxides amount keeps low fraction (≈0.5 wt%) within the film. However, about 180% absorption enhancement was observed, when the Ag@oxides amount is 0.5 wt%. Photoluminescence (PL) results indicate that the ultrathin (1–2 nm) oxides layer can effectively prevent from the recombination of photo-generated charges and further boost the PCE of PV devices. Femtosecond-transient absorption spectroscopy (fs-TAS) results indicate that the photo-induced absorption (PIA) band, which stands for polaron pair generation, becomes more efficient in Ag@oxides blended P3HT films. PL and PIA decay spectra results indicate that the ultrathin oxide shell can efficiently prevent the exciton from recombination. The PV devices of P3HT:PCBM blended with Ag@oxides were fabricated. About 31% PCE enhancement was observed due to the addition of Ag@oxides nanoprisms, which is higher than previous reports.[6b,12]

2. Results and Discussion

2.1. Synthesis and Functionalization of Ag@TiO_2 and Ag@SiO_2 Core–Shell Nanoprisms

The Ag@oxides core–shell nanostructures were synthesized using a stepwise synthetic protocol as in our previous reports.[11,13] In previous works, it was easy to get the ultrathin oxides shell, e.g., TiO_2 and SiO_2 by controlling the reaction time and the amount of the reactant, respectively. To obtain maximum absorption band overlap between Ag nanoprisms and P3HT, the size of Ag nanoprisms were controlled within 20–25 nm of side length. The corresponding LSPR absorption band of Ag nanoprism locates at ≈450 nm. Transmission electron microscopy (TEM) images of core–shell Ag@oxides nanostructures, as shown in **Figure 1**A,B, exhibit that Ag nanoprisms are coated with a very thin layer of TiO_2 or SiO_2 shell with thickness of 1.0–1.5 nm. The distinct boundary between Ag nanoprisms and oxides is clearly visible due to a large difference in electron density between the crystalline Ag nanoprisms and the amorphous oxide shell. The LSPR absorption band of Ag nanoprisms shifts from ≈450 to ≈490 nm after coating the oxides, having higher dielectric constant than the surrounding liquid.

To improve the solubility of Ag@oxides nanoprisms in organic solvent, like 1,2-dichlorobenzene (1,2-DCB), two routes are employed. One is adsorbing alkyl amine molecules on the Ag@TiO_2 surface, another is introducing methyl group on the surface of Ag@SiO_2 nanoprisms by adding methyltriethoxysilane (MTES) into the sol–gel reaction. These modifications result in Ag@oxides nanoprisms well dispersed in 1,2-DCB. (Figure S1, Supporting Information). Fourier transform-infrared (FT-IR) spectra (Figure 1D) were used to identify the surface functional groups adsorbed on Ag@TiO_2 nanoprisms surface. The broad absorption peak at 3000–3500 cm^{-1} are assigned to stretching vibrations of N–H in amine molecules. The peaks at 2861 and 2916 cm^{-1} are assigned to CH_2 characteristic peaks. These results indicate that amine molecules anchor on the surface of Ag@TiO_2 nanoprisms. Figure 1C shows the UV–vis absorption spectra of Ag@TiO_2–hexylamine (HA), Ag@TiO_2–dodecylamine (DA), and Ag@TiO_2–octadecylamine (ODA) colloids in 1,2-DCB. The corresponding LSPR adsorption band shifts to 508, 518, and 525 nm for Ag@TiO_2–HA, DA, and ODA in 1,2-DCB solution, respectively. The redshift of LSPR band attributes that 1,2-DCB has higher refraction index than ethanol. For the Ag@SiO_2 nanoprisms, the surface functionalization of the Ag@SiO_2 core–shell nanoprisms is implemented by hydrolysis of MTES and left Si–CH_3 groups on the Ag@SiO_2 nanoprisms surface.

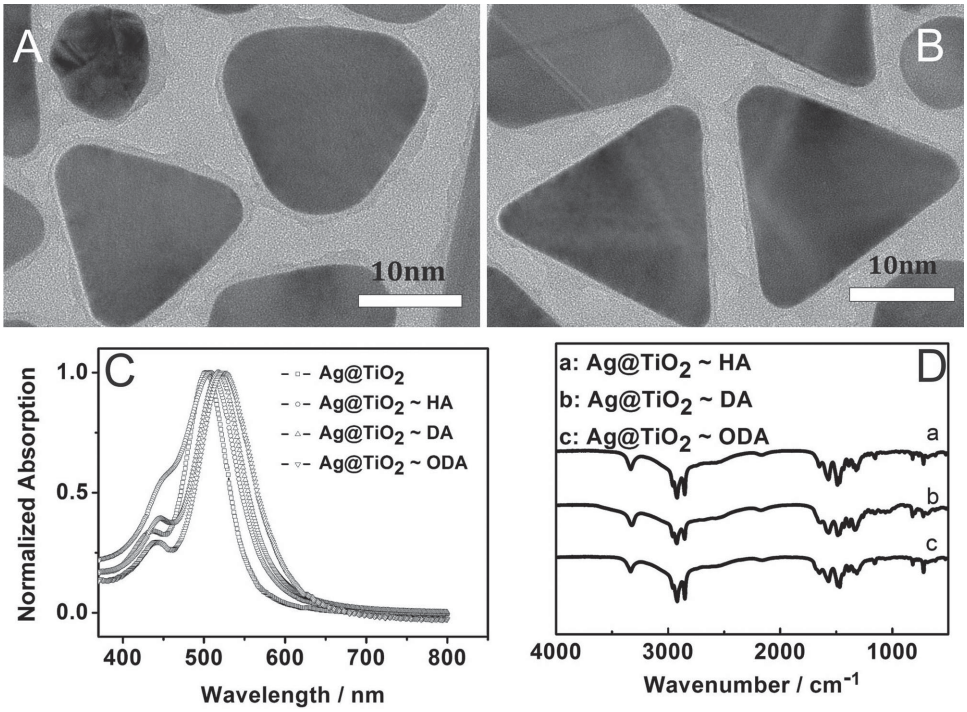

Figure 1. TEM images of $Ag@TiO_2$ A) and $Ag@SiO_2$ B) nanoprisms. Normalized UV–vis absorption spectra $Ag@TiO_2$, and $Ag@TiO_2$–HA, DA and ODA in 1,2-DCB solution C) and FT-IR spectra D) of the different alkylamine functionalized $Ag@TiO_2$ nanoprisms.

2.2. Effect of LSPR on the Steady-State Spectroscopy of the P3HT Thin Film

As we know, the PCE of polymer solar cells strongly depends on the morphology of active layer. AFM images, as shown in Figure S2 (Supporting Information), exhibit the morphology of P3HT with different amount of Ag@oxides nanoprisms. The lamellar structures are observed in Figure S2 (Supporting Information) due to the self-assembly behavior of P3HT. The lamellar structure gradually turns into aggregated NPs with increasing amount of Ag@oxides in the blend system. To avoid the effect of morphology change of active layer, the concentration of these Ag@oxides core@shell particles was limited within very low fraction from 0.3 wt%, 0.5 wt% to 1.0 wt% for this work. Each film was prepared by spin-coating the mixture of P3HT and Ag@oxides solution on the substrate at 700 rpm for 1 min. The pristine P3HT film was also prepared as a reference. The UV–vis absorption spectra of P3HT and Ag@oxides blended films are shown in **Figure 2**. The absorption spectra of P3HT blended with different amount of the Ag@oxides core–shell nanoprisms exhibit similar absorbance features. Normally, the absorption band at 620 nm stands for the self-assembly of P3HT chain.[14] The peak at 620 nm indicates that both pristine P3HT and blended P3HT/Ag@oxides have a good self-assembly behavior with ignorable change. The black and red lines in Figure 2A–E stand for the absorption of pristine P3HT and the P3HT/Ag@oxides core@shell nanoprisms thin film on the bare glass substrate. The net enhancement of the P3HT absorption (difference spectrum, green line) is obtained by subtracting the absorption of pure P3HT from the absorption of the blending one. The absorption enhancement rate (AER) is calculated from the ratio of the inner area of the difference spectrum and that of P3HT. Figure 2A–C shows that the absorption spectra of P3HT film with the presence of 0.3–1.0 wt% $Ag@TiO_2$–HA nanoprisms. The maximum relative absorption enhancement of P3HT occurs at 560 nm (Figure 2A, red line). Approximately 65% AER is obtained when P3HT is blended with 0.3 wt% of the $Ag@TiO_2$–HA nanoprisms. This result is obviously better than our previous report.[11] When the amount of $Ag@TiO_2$–HA nanoprisms reaches 0.5 wt%, the AER reaches 110%. This increase in the absorption enhancement of P3HT could be attributed to the interaction between the P3HT and the enhanced electric field surrounding the $Ag@TiO_2$ NPs, which was known as LSPR. On one hand, the more $Ag@TiO_2$ NPs is added into, the more site generates LSPR, the stronger electric field will be generated by near-field coupling each other. On the other hand, Ag@oxides nanoprisms could be worked as scattering centers, which could directly lead to the increase of the optical path length in the P3HT film, improving the utilization of P3HT for the incident light. However, when introducing more $Ag@TiO_2$ NPs–HA (≈1.0 wt%) to the P3HT film, the AER drops down to ≈88%. It may be affected by the morphology change of P3HT due to too many NPs. Compared to the pristine P3HT film, the maximum AER of the P3HT film incorporated with $Ag@TiO_2$–DA, $Ag@TiO_2$–ODA, and $Ag@SiO_2$–MTES at the weight ratio of 0.5 wt% are 130%, 180%, and 150%, repectively. Figure S3 (Supporting Information) shows the absorption enhancement when Ag@oxides are embedded into the P3HT:PCBM OPV devices. $Ag@TiO_2$–ODA also display the highest enhancement for the absorption.

Steady-state PL could give a deep understanding on the effect of LSPR on the exciton generation behavior, and the

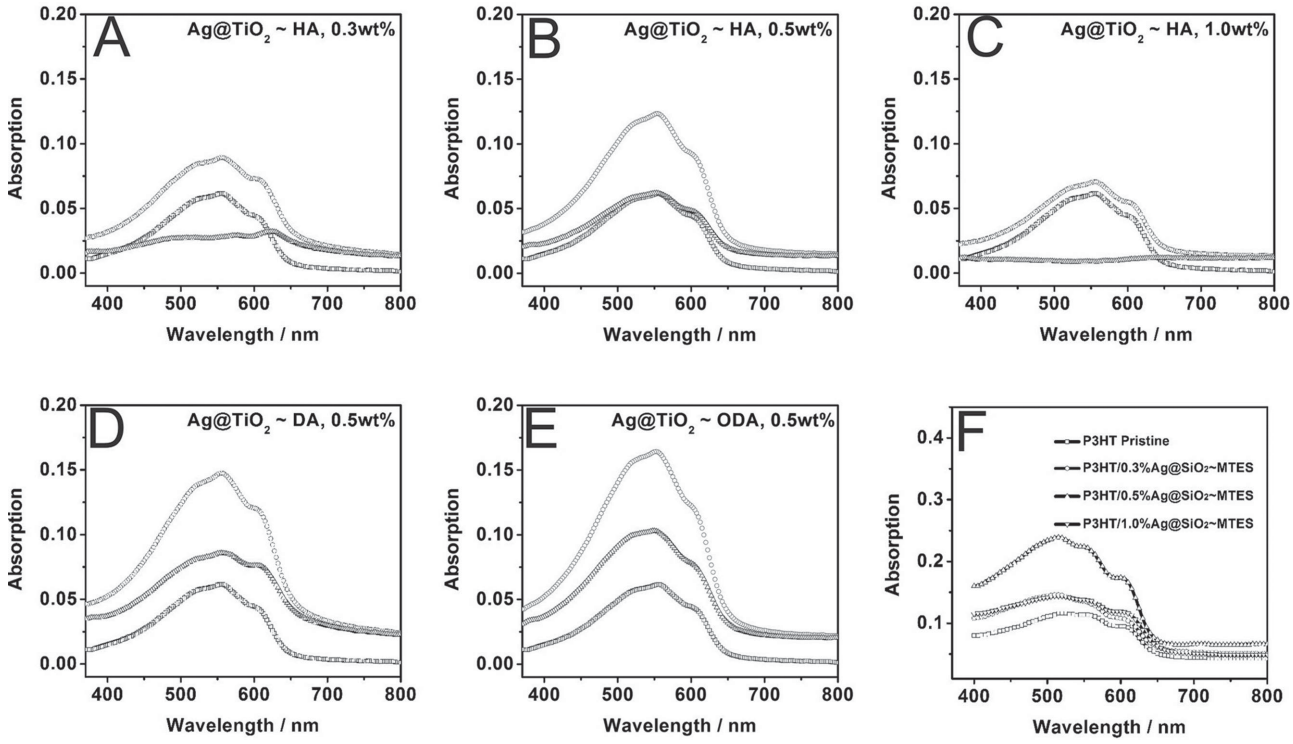

Figure 2. The LSPR-PIA enhancement of the P3HT thin film, blended with different amount of Ag@TiO_2–HA (A, 0.3 wt%; B, 0.5 wt%; and C, 1.0 wt%); D, 0.5 wt% Ag@TiO_2–DA; E, 0.5 wt% Ag@TiO_2–ODA. The optical absorption of pristine P3HT (black), Ag@TiO_2/P3HT (red), and the difference (green) on bare glass. Difference (ΔAb) = Ag@TiO_2/P3HT (red)–pristine P3HT (black). F is the UV–vis absorption spectra of P3HT with different amount of Ag@SiO_2 nanoprisms.

exciton in the active layer is predominately created from the absorption of the donor. The steady-state PL spectra were measured using a Xenon lamp as the excitation source (λ = 550 nm). **Figure 3**A displays PL spectra of P3HT with different amount of Ag@TiO_2–ODA. The PL intensity at the peak of 640 nm increased as much as approximately fourfold after incorporating 0.5 wt% of the Ag@TiO_2–ODA nanoprisms. PL intensity decreases when the amount of Ag@TiO_2–ODA further increase to 1.0 wt%, that may cause from the morphology change of P3HT film due to the addition of excess amount Ag@TiO_2–ODA. Similar results were observed for the P3HT/Ag@SiO_2 nanoprisms case (Figure S4, Supporting Information). However, equal amount Ag nanoprisms capped with thiol group are added into P3HT film, the PL intensity of P3HT declines ≈50% compared with that of pristine P3HT. These results imply that the TiO_2 shell can effectively prevent from the exciton recombination happened on the Ag nanoprisms site. When introducing Ag@TiO_2–ODA nanoprisms to the blending film P3HT:PCBM, the PL intensity declines to some extent (Figure 3B), indicating charge separation at the interface of P3HT and PCBM is enhanced in this case. These phenomenon are observed in the case of embedding the Ag@oxides into the active layer of P3HT:PCBM OPV device (Figure S5, Supporting Information). These results indicate that the LSPR of Ag@TiO_2 changes the electric field around Ag NP. High energy field may promote the exciton

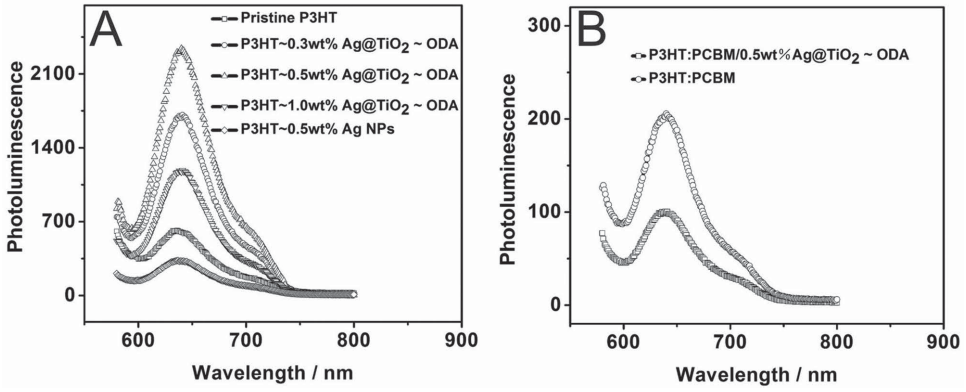

Figure 3. The PL spectra of P3HT with Ag and different amount Ag@TiO_2–ODA nanoprisms A) and P3HT:PCBM, P3HT:PCBM/Ag@TiO_2–ODA B) on bare glass.

dissociation at the interface of P3HT and PCBM, resulting in the decrease of P3HT PL intensity.

2.3. Effect of LSPR on the Transient Absorption Spectroscopy of the P3HT Thin Film

Here, to better understand and compare the physical–chemical properties taking place upon blending, we investigated the photophysics of (i) P3HT film; (ii) P3HT blending with Ag@oxides nanoprisms; (iii) P3HT:PCBM film; and (iv) P3HT:PCBM blending with Ag@oxides nanoprisms (Figures S6–S13, Supporting Information). We directly probe transient absorption spectroscopy with an ultrafast pump probe system with time delays ranging from 100 fs to 200 ps, driven by 10 μJ, 150 fs pulses at 1 kHz repetition rate and 800 nm wavelength. The pump beam at $\lambda = 400$ nm provides spanning in the 420–735 nm range.

Wu et al. investigated the OPV device using P3HT:PCBM blended with oleylamine-capped Ag NPs as active layer by femtosecond-transient absorption spectroscopy (fs-TAS).[10a] Although an initial increase of exciton generation promoted by the presence of silver NPs, the high trapping rate of the generated polarons limits the amount of free carriers in the hybrid systems. The Ag NPs promote trap-assisted recombination and degrade the performance of the hybrid plasmonic OPVs. Here, the addition of ultrathin layer of oxides is expected to depress trap-assisted recombination. **Figure 4** shows fs-TAS spectra of pristine P3HT film and P3HT:PCBM film ranging from 200 fs to 100 ps time delay. The pristine crystalline-P3HT film (Figure 4A) exhibits a positive signal below 630 nm with three distinct vibronic peaks at 610 (0–0), 560 (0–1), and 520 nm (0–2) (in order of increasing energy), assigned to ground-state bleaching (GSB) peaks.[15] The relative prominence of the 610 nm (0–0) peak is consistent with a good degree of P3HT ordering, as expected in P3HT only film and other.[14] There is a very weak negative band between 700 and 735 nm arising from the stimulated emission (SE) of singlet excitons, and negative feature with a peak centered at 660 nm is PIA,[16] which attributed to small populations of charge pairs that we find to be directly photogenerated. Its shape and close proximity to the GSB features, and the shape of the PIA peak is also clearly affected by the overlap of GSB and SE associated with excitons. Normally, there are two bands at 660 and 1100 nm associated to the PIA for P3HT samples. Korovyanko et al. pointed out that the low energy and high energy PIA in P3HT are likewise due to excitons and geminate polaron pairs, respectively.[17] We focus on the PIA band at 660 nm in this text. Figure 4B,C shows the representative differential transmission signals at 200 fs and 1 ps delay for the P3HT (black line) and P3HT with 0.5 wt% Ag@TiO_2–ODA(red line), respectively. The absolute magnitudes of PIA band at 660 nm are more pronounced in the P3HT/Ag@TiO_2–ODA than that in pure P3HT. It is found that an estimated increase of ≈50- and ≈40-folds results for the 200 fs and 1 ps delay, respectively. That indicates that polaron pair generation is more efficient in P3HT blended with Ag@TiO_2–ODA films than that in pure P3HT film (Figure 4B). Since the polymer chains in the lamellae have longer conjugation and smaller interchain distance,[16b]

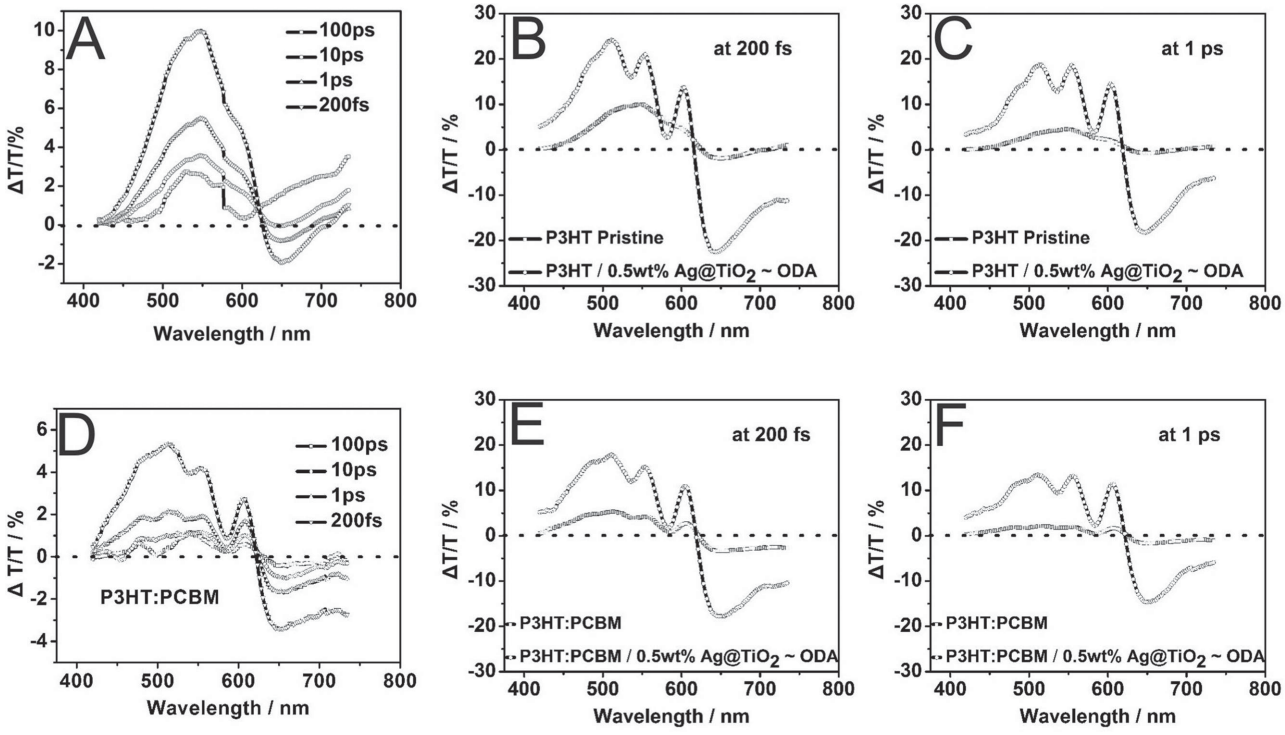

Figure 4. The effect of Ag@TiO_2–ODA on the exciton and polaron generation observed via Femtosecond transient absorption spectroscopy. Relative differential transmission ($\Delta T/T$) of P3HT A–C) and P3HT:PCBM D–F) film ranged from 420 to 735 nm. Selected times are 200 fs and 1 ps after excitation with 400-nm laser beam.

the oscillation of the electromagnetic field by introducing the Ag NPs may cause stronger interchain–interlayer interaction. So the "contact points" between any two adjacent chains are therefore more extended. Moreover, the extended "contact points" for the polymer chains in the adjacent lamellae leads to more mobile polaron pairs in P3HT. So, the increased interlayer–interchain coupling in the lamellae causes excess broadening to their optical transitions, resulting in the states split, and then PIA band broaden in the blended thin films as observed (Figure 4B,C,E,F). These indicate that the rate of singlet exciton generation is indeed enhanced with the presence of the Ag@TiO_2–ODA nanoprisms. Also, we could find the same broaden PIA band in the case of P3HT:PCBM/Ag@TiO_2–ODA (Figure 4E,F). The differential transmission signal intensity in P3HT:PCBM (Figure 4D–F) cases are lower than that in P3HT films (Figure 4A–C), because the PCBM as electron acceptor promote the exciton dissociation, which leads to the concentration of exciton decrease to some extend. On the basis of fs-TAS results, the increasing exciton concentration is observed in both P3HT and P3HT:PCBM blended with Ag@oxides cases.

To better comprehend the initial state of excitations in P3HT, which is revealed in the ultrafast PIA spectra, we studied the transient dynamics of high energy PIA band comparing with the reference samples. **Figure 5** shows the decay transients of the PIA band signals at 660 nm for the references and P3HT/Ag@oxides sample. For pristine P3HT sample, the lifetime decay of polaron is quickly decay off, indicating a short lifetime for polaron in P3HT. When the bare Ag nanoprisms were introduced into the system, fast decay and short lifetime are close to the pure P3HT, which is consistent with Wu's report. It indicates that trap-assisted recombination limit the amount of free carriers in the hybrid systems.[10a] However, when Ag@oxides blend with P3HT, the PIA decay exhibits much slower relaxations. It indicates that the photogenerated exciton has a longer lifetime in the P3HT/Ag@oxides hybrid film. That implies that oxides layer can effectively prevent from the trap-assisted recombination of photogenerated exciton

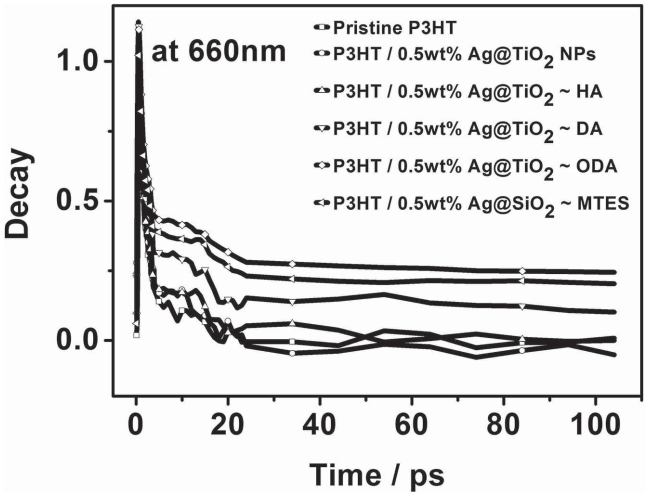

Figure 5. Transient decays of P3HT film, P3HT blended with Ag NPs and P3HT blended with Ag@oxides nanoprisms. PIA decay monitored at 660 nm.

of P3HT. Similar results were observed in the P3HT:PCBM/Ag@oxides and OPV device cases (Figures S12 and S13, Supporting Information). The LSPR effect of Ag nanoprism will generate an enhanced electric field around the Ag nanoprism. This high energy field promotes the surrounding media to absorb more light and keep the exciton in long lifetime. In a word, the addition of Ag@oxides could enhance the generation and the lifetime of exciton, the oxide shell effectively depresses the recombination rate comparing to the bare Ag NPs.

2.4. Effect of LSPR on the OPVs

To demonstrate the plasmonic effect of Ag@oxides nanoprisms on OPV devices, we designed a series of PV devices as shown in **Figure 6**A. The control device with the structure of ITO/TiO_2 layer/P3HT:PCBM/MoO_3/Ag, was measured at the same conditions. The effect of 0.5 wt% Ag@TiO_2–ODA NPs on the OPV devices performance is shown in Figure 6B,C, and detailed data are summarized in **Table 1** and Figure S14 (Supporting Information). The control device display open-circuit voltage (V_{OC}) of 0.59 V, short-circuit current (J_{SC}) of 9.67 mA cm^{-2}, fill factor (FF) of 0.54, and PEC of 3.10%. When bare Ag nanoprisms capped with thiol group were added into the active layer —P3HT:PCBM, J_{SC}, and FF decrease to 6.60 and 0.45 mA cm^{-2}, resulting in a low PCE = 1.69. When Ag@TiO_2–HA and DA were introduced into the PV devices, the J_{SC} increases about 1.0 mA cm^{-2} and FF slightly decreases to 0.51. The PCE of P3HT:PCBM/Ag@TiO_2–HA and DA show slightly high value as that of control sample. The P3HT/PCBM OPV device with 0.5 wt% Ag@TiO_2–ODA NPs exhibits better performance, such as PEC of 4.03%, V_{OC} = 0.58 V, J_{SC} = 13.76 mA cm^{-2}, and FF = 0.51, respectively (Figure 6B,C, red line). The best device shows PCE of 4.15%. From the above data, the PCE enhancement of device mainly contributes from the increase of J_{SC}, which changes from 9.67 to 13.76 mA cm^{-2}, leading to a 31% increase of PCE. It should be noted that the series resistance (R_S) of devices shows a slight increase when adding Ag@oxides NPs into the active layer. That is the reason why FF decreases from 0.54 to 0.51.

The incident photon-to-current efficiency (IPCE) measurement was performed to study the effect of LSPR on the spectral response of solar cells. The IPCE directly reflects the active layer in solar cell for the response of the incident light in different wavelength position. As shown in Figure 6C, the Ag@TiO_2–ODA NPs blended device has a remarkable higher IPCE than the reference device, corresponding to the increase of J_{SC}. Besides, the difference spectrum (Figure 6D) between the two in Figure 6C covers the whole P3HT absorption band from 400 to 620 nm, and its shape is very similar to the absorption enhancement of the P3HT thin film (Figure 3). This indicates that the LSPR enhancement could cover the whole P3HT absorption range. The IPCE enhancement is about 23.9% related to the control device. Based on these results, we infer that the LSPR effect is the main contributor for PCE enhancement in the case of P3HT:PCBM blended with Ag@TiO_2–ODA.

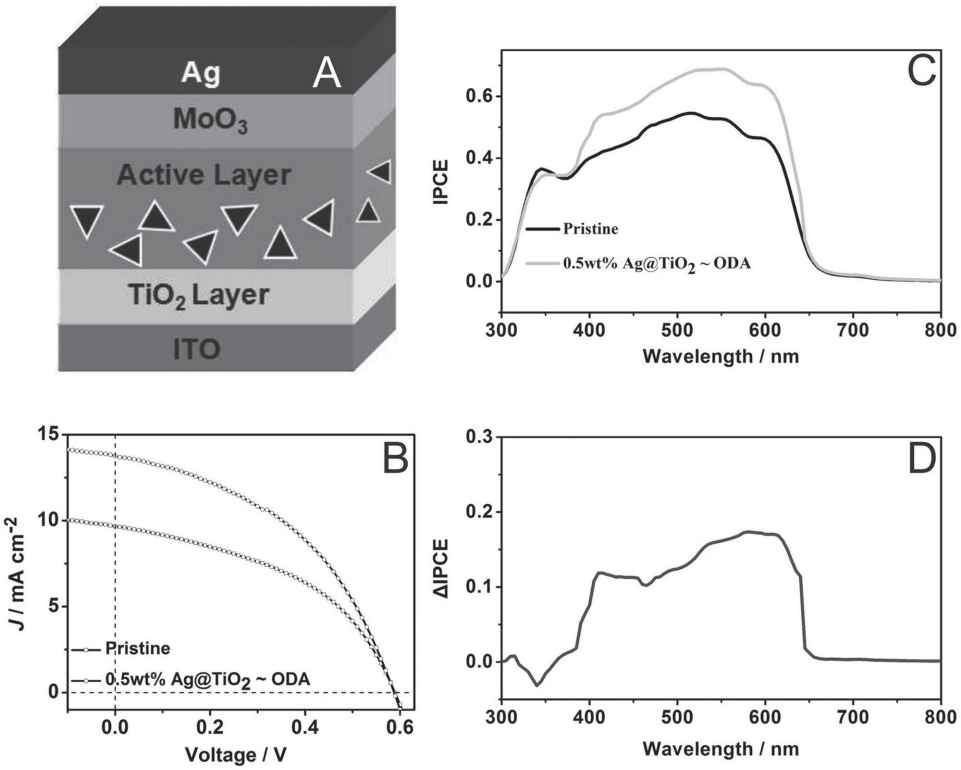

Figure 6. Schematic device structures of the solar cells used in this work A). Current–voltage characteristics of OPVs with and without 0.5 wt% Ag@TiO_2–ODA nanoprisms B). IPCE spectra of the OPVs with and without 0.5 wt% Ag@TiO_2–ODA nanoprisms C). The relative change of the IPCE caused by the incorporation of Ag@TiO_2–ODA nanoprisms. $\Delta IPCE = IPCE_{plasmon\text{-}enhanced}(\lambda) - IPCE_{ref}(\lambda)$ D).

3. Conclusion

In summary, alkyl groups surface modified Ag@oxides nanoprisms were prepared and successfully added into the polymer photovoltaic device active layer. We systemically investigated the LSPR effect of Ag@oxides on the P3HT, P3HT:PCBM thin film, and P3HT:PCBM PV devices. UV–vis absorption spectra show significant absorption enhancement (≈180%) even the Ag@oxides amount was limited within a very small fraction region (0.3–1.0 wt%). PL results imply that oxides layer efficiently prevents the photogenerated exciton from recombination. fs-TAS results display that the PIA band dramatically increases due to the addition of Ag@oxides. The relaxation time of photogenerated polaron in the polymer (P3HT and P3HT:PCBM) with Ag@oxides is much longer than that in polymer. It indicates that the LSPR effect enhances the absorption of P3HT and makes a photogenerated polaron long lifetime, which is beneficial to the charge separation. Finally, we fabricated the PV device with the addition of Ag@oxides into the active layer. The incorporation of Ag@TiO_2–ODA nanoprisms into the P3HT:PCBM-based OPVs remarkably improves device performance, resulting in a PCE of 4.03% via additional light absorption and scattering effects over a broad spectral range of 400–620 nm.

Table 1. Photovoltaic parameters of solar cells with different NPs under AM 1.5G illumination at 100 mW cm^{-2}.

NPs	J_{SC} [mA cm^{-2}]	V_{OC} [V]	FF [%]	R_s [Ωcm^{-2}]	PCE [%]
No	9.67	0.59	0.54	20	3.10
Ag NPs thiol	6.60	0.57	0.45	40	1.69
Ag@TiO_2–HA	10.45	0.59	0.51	29	3.13
Ag@TiO_2–DA	10.72	0.59	0.52	26	3.29
Ag@TiO_2–ODA	13.76	0.58	0.51	30	4.03(4.15[a)])
Ag@SiO_2–MTES	11.16	0.58	0.51	31	3.30

[a)]Best device.

4. Experimental Section

Chemicals: Poly(sodium styrene sulfonate) (PSSS, 25 wt% solution in water, M_w = 10 00 000) was purchased from Sigma-Aldrich. Silver nitrate, H_2O_2, NaCl, and *n*-propanol were purchased from Beijing Chemical Co. Tetrabutyl titanate (TBT) (AR grade), tetraethyl orthosilicate (TEOS), sodium citrate, and $NH_3 \cdot H_2O$ were obtained from Tianjin Guangfu Fine Chemical Research Institute. Sodium borohydride was purchased from Sinopharm Chemical Reagent Co. Ascorbic acid, *N*-hexylamine, DA, ODA, and MTES were purchased from Aladdin Industrial Corp. 1,2-dichlorobenzene was purchased from Acros Organics. All the chemicals were used without further purification. Deionized (DI) water was purified through a Milli-Q water purification system, and the resistivity was 18.2 MΩ cm.

Synthesis of Ag Nanoprisms: The Ag nanoprisms were synthesized using a seed-mediated procedure with a few modifications.

First, aqueous sodium citrate (22.5 mL, 2.5×10^{-3} M), aqueous poly(sodium styrene sulfonate) (PSSS, 2.5 mg), and aqueous $NaBH_4$ (1.5 mL, 10×10^{-3} M, freshly prepared and cooled at 0 °C) were mixed together successively followed by addition of aqueous $AgNO_3$ (22.5 mL, 0.5×10^{-3} M) at a rate of 2 mL min^{-1} while the mixture was being continuously stirred. Then the yellow solution of Ag seeds was obtained. Second, 45 mL of ultrapure water was mixed with aqueous L-ascorbic acid (0.675 mL, 10×10^{-3} M) and 1.2 mL of the seed solution, followed by the mixture being dropped into aqueous $AgNO_3$ (27 mL, 0.5×10^{-3} M) at a rate of 1 mL min^{-1}. After that, aqueous trisodium citrate (5 mL, 25×10^{-3} M) was injected to stabilize the nanoprisms. Under magnetic stirring, the color of the solution changed gradually during the dropping of the $AgNO_3$ solution and was finally stable at orange (the peak of the LSPR band at 470 nm). The product was directly used for Ag@oxides core–shell nanoprisms without further purification.

Synthesis of Ag@TiO_2 Core–Shell Nanoprisms: Citric acid (32 mg) was dissolved in 10 mL of *n*-propanol, and then TBT (0.34 g) was added to the citric acid solution. After the mixture had been stirred for 30 min, the TiO_2 sol–gel precursor was filtered with a syringe filter (0.22 μm) for coating Ag nanoprisms. The stock Ag nanoprisms solution (10 mL) was mixed with 20 μL of 0.7 g mL^{-1} aqueous citrate acid, and then 20 μL of the TiO_2 sol–gel precursor was injected while the mixture was being vigorously stirred for 3 h. The thickness of the TiO_2 shell can be tuned by changing the reaction time. Finally, the reaction product was isolated by centrifugation at 10 000 rpm for 20 min at 4 °C to remove excessive TiO_2 sol–gel precursor. The precipitate was redispersed in ethanol, and the washing steps were repeated 3× to obtain clean Ag@TiO_2 nanoprisms.

Synthesis of Ag@SiO_2 Core–Shell Nanoprisms: The SiO_2 sol–gel precursor was obtained by mixing successively ethanol, DI water, $NH_3 \cdot H_2O$, and tetraethyl orthosilicate (TEOS) in a volume ratio of 184:15:1:0.3. Then, 100 mL of the SiO_2 sol–gel precursor was mixed with 20 mL of a Ag nanoprism solution while the mixture was vigorously stirred for at least 5 h. The thickness of the SiO_2 shell can be tuned by changing the reaction time. Finally, the reaction product was isolated by centrifugation at 10 000 rpm for 20 min at 4 °C, and the precipitate was redispersed in ethanol. The washing steps were repeated 3× to obtain clean Ag@SiO_2 nanoprisms.

Surface Functionalization of Ag@Oxides Core–Shell Nanoprisms: Briefly, 1 mL of 50 wt% Ag@TiO_2 nanoprisms were added in 20 mL of 20 mg mL^{-1} *N*-hexylamine (DA, ODA) dissolved in chloroform under strong stirring for more than 12 h, and then centrifuged at 7000 rpm for 10 min at 4 °C to remove excessive *N*-hexylamine (DA, ODA), chloroform, and ethanol. Finally, the precipitate was redispersed in 1,2-dichlorobenzene. For Ag@SiO_2–MTES, 1 mL of 50 wt% Ag@SiO_2 nanoprisms were added in 20 μL $NH_3 \cdot H_2O$ (32%), and then added drop-wise MTES slowly under strong stirring over more than 12 h, and then centrifuged at 7000 rpm for 10 min at 4 °C to remove excessive MTES and H_2O, the precipitate was redispersed in 1,2-dichlorobenzene.

Characterization: The absorption spectra were recorded with a UV–vis absorption spectrometer (Shimadzu UV-2600). Fluorescence emission spectra were recorded on a F4500 fluorophotometer. Transmission electron microscopy (TEM) images were obtained with a FEI Tecnai G2 TEM operating at 200 kV, obtained using a FEI Tecnai G2 operated at 200 kV. The size of the Ag@SiO_2 and the Ag@TiO_2 core–shell NPs was obtained from TEM images by counting over 100 individual particles. Atomic force microscopy (AFM) images were captured on the Multimode 8 (Bruker Co.) in tapping mode. Fourier transform-infrared (FT-IR) spectra were recorded using KBr pellets with a Bruker Vertex 70 spectrometer from 4000 to 470 cm^{-1}. A Zolix Solar cell Scan 100 was used for measuring IPCE values. A Keithley 2400 was used for recording *J–V* characteristics.

Supporting Information

Supporting Information is available from the Wiley Online Library or from the author.

Acknowledgements

This work was supported by the National Natural Science Foundation of China (Grant Nos. 61306081 and 61176016) and the Natural Science Foundation of Jilin Province (Grant No. 20130522142JH,). Z.S. thanks the support of the "Hundred Talent Program" of CAS, and Innovation and Entrepreneurship Program of Jilin.

[1] a) N. S. Sariciftci, L. Smilowitz, A. J. Heeger, F. Wudl, *Science* **1992**, *258*, 1474; b) G. Yu, J. Gao, J. C. Hummelen, F. Wudl, A. J. Heeger, *Science* **1995**, *270*, 1789; c) J. J. M. Halls, C. A. Walsh, N. C. Greenham, E. A. Marseglia, R. H. Friend, S. C. Moratti, A. B. Holmes, *Nature* **1995**, *376*, 498.

[2] a) Y. Y. Liang, Z. Xu, J. B. Xia, S. T. Tsai, Y. Wu, G. Li, C. Ray, L. P. Yu, *Adv. Mater.* **2010**, *22*, E135; b) C. Piliego, T. W. Holcombe, J. D. Douglas, C. H. Woo, P. M. Beaujuge, J. M. J. Frechet, *J. Am. Chem. Soc.* **2010**, *132*, 7595.

[3] a) X. M. He, F. Gao, G. L. Tu, D. Hasko, S. Huttner, U. Steiner, N. C. Greenham, R. H. Friend, W. T. S. Huck, *Nano Lett.* **2010**, *10*, 1302; b) J. Y. Kim, K. Lee, N. E. Coates, D. Moses, T. Q. Nguyen, M. Dante, A. J. Heeger, *Science* **2007**, *317*, 222.

[4] a) X. N. Yang, J. Loos, S. C. Veenstra, W. J. H. Verhees, M. M. Wienk, J. M. Kroon, M. A. J. Michels, R. A. J. Janssen, *Nano Lett.* **2005**, *5*, 579; b) J. Peet, J. Y. Kim, N. E. Coates, W. L. Ma, D. Moses, A. J. Heeger, G. C. Bazan, *Nat. Mater.* **2007**, *6*, 497; c) J. M. Lobez, T. L. Andrew, V. Bulovic, T. M. Swager, *ACS Nano* **2012**, *6*, 3044.

[5] a) J. B. You, L. T. Dou, K. Yoshimura, T. Kato, K. Ohya, T. Moriarty, K. Emery, C. C. Chen, J. Gao, G. Li, Y. Yang, *Nat. Commun.* **2013**, *4*, 1446; b) Y. S. Liu, C. C. Chen, Z. R. Hong, J. Gao, Y. Yang, H. P. Zhou, L. T. Dou, G. Li, Y. Yang, *Sci. Rep.* **2013**, *3*, 3356; c) J. Jo, J. R. Pouliot, D. Wynands, S. D. Collins, J. Y. Kim, T. L. Nguyen, H. Y. Woo, Y. M. Sun, M. Leclerc, A. J. Heeger, *Adv. Mater.* **2013**, *25*, 4783.

[6] a) S. H. Park, A. Roy, S. Beaupre, S. Cho, N. Coates, J. S. Moon, D. Moses, M. Leclerc, K. Lee, A. J. Heeger, *Nat. Photonics* **2009**, *3*, 297-U5; b) D. H. Wang, D. Y. Kim, K. W. Choi, J. H. Seo, S. H. Im, J. H. Park, O. O. Park, A. J. Heeger, *Angew. Chem Int. Ed.* **2011**, *50*, 5519.

[7] a) H. A. Atwater, A. Polman, *Nat. Mater.* **2010**, *9*, 205; b) Q. Gan, F. J. Bartoli, Z. H. Kafafi, *Adv. Mater.* **2013**, *25*, 2385.

[8] a) K. L. Kelly, E. Coronado, L. L. Zhao, G. C. Schatz, *J. Phys. Chem. B* **2003**, *107*, 668; b) I. Pastoriza-Santos, L. M. Liz-Marzan, *J. Mater.*

Chem. **2008**, *18*, 1724; c) X. M. Lu, M. Rycenga, S. E. Skrabalak, B. Wiley, Y. N. Xia, *Annu. Rev. Phys. Chem.* **2009**, *60*, 167.

[9] a) L. Y. Lu, Z. Q. Luo, T. Xu, L. P. Yu, *Nano Lett.* **2013**, *13*, 59; b) M. Salvador, B. A. MacLeod, A. Hess, A. P. Kulkarni, K. Munechika, J. I. L. Chen, D. S. Ginger, *ACS Nano* **2012**, *6*, 10024; c) D. D. S. Fung, L. F. Qiao, W. C. H. Choy, C. D. Wang, W. E. I. Sha, F. X. Xie, S. L. He, *J. Mater. Chem.* **2011**, *21*, 16349; d) F. C. Chen, J. L. Wu, C. L. Lee, Y. Hong, C. H. Kuo, M. H. Huang, *Appl. Phys. Lett.* **2009**, *95*, 013305; e) C. C. D. Wang, W. C. H. Choy, C. H. Duan, D. D. S. Fung, W. E. I. Sha, F. X. Xie, F. Huang, Y. Cao, *J. Mater. Chem.* **2012**, *22*, 1206.

[10] a) B. Wu, X. Y. Wu, C. Guan, K. F. Tai, E. K. L. Yeow, H. J. Fan, N. Mathews, T. C Sum, *Nat. Commun.* **2013**, *4*, 2004; b) K. Topp, H. Borchert, F. Johnen, A. V. Tune, M. Knipper, E. von Hauff, J. Parisi, K. Al-Shamery, *J. Phys. Chem. A* **2010**, *114*, 3981; c) M. Xue, L. Li, B. J. T. de Villers, H. J. Shen, J. F. Zhu, Z. B. Yu, A. Z. Stieg, Q. B. Pei, B. J. Schwartz, K. L. Wang, *Appl. Phys. Lett.* **2011**, *98*, 253302.

[11] P. Du, Y. H. Cao, D. Li, Z. Y. Liu, X. G. Kong, Z. C. Sun, *RSC Adv.* **2013**, *3*, 6016.

[12] a) B. V. K. Naidu, J. S. Park, S. C. Kim, S. M. Park, E. J. Lee, K. J. Yoon, S. J. Lee, J. W. Lee, Y. S. Gal, S. H. Jin, *Sol. Energy Mater. Sol. Cells.* **2008**, *92*, 397; b) D. H. Wang, K. H. Park, J. H. Seo, J. Seifter, J. H. Jeon, J. K. Kim, J. H. Park, O. O. Park, A. J. Heeger, *Adv. Energy Mater.* **2011**, *1*, 766; c) X. H. Li, W. C. H. Choy, H. F. Lu, W. E. I. Sha, A. H. P. Ho, *Adv. Funct. Mater.* **2013**, *23*, 2728.

[13] P. Du, L. Ma, Y. H. Cao, D. Li, Z. Y. Liu, Z. X. Wang, Z. C. Sun, *ACS Appl. Mater. Inter.* **2014**, *6*, 8853.

[14] a) F. C. Spano, *J. Chem. Phys.* **2005**, *122*, 234701; b) Clark, C. Silva, R. H. Friend, F. C. Spano, *Phys. Rev. Lett.* **2007**, *98*, 206406.

[15] R. A. Marsh, J. M. Hodgkiss, S. Albert-Seifried, R. H. Friend, *Nano. Lett.* **2010**, *10*, 923.

[16] a) R. Mauer, I. A. Howard, F. Laquai, *J. Phys. Chem. Lett.* **2010**, *1*, 3500; b) X. M. Jiang, R. Osterbacka, O. Korovyanko, C. P. An, B. Horovitz, R. A. J. Janssen, Z. V. Vardeny, *Adv. Funct. Mater.* **2002**, *12*, 587.

[17] O. J. Korovyanko, R. Osterbacka, X. M. Jiang, Z. V. Vardeny, R. A. J. Janssen, *Phys. Rev. B* **2001**, *64*, 235122.

Received: September 12, 2014
Revised: November 1, 2014
Published online: January 15, 2015